Thermal Science and Engineering Progress 42 (2023) 101926

Contents lists available at ScienceDirect

Thermal Science and Engineering Progress

journal homepage: www.sciencedirect.com/journal/thermal-science-and-engineering-progress

An innovative PDMS cell to improve the thermal conductivity measurements of nanofluids

R.R. Souza [a,*], F.M. Sá Barbosa [a], G. Nobrega [a], E.M. Cardoso [b,c], J.C.F. Teixeira [a], A.S. Moita [d,e], R. Lima [a,f]

[a] Metrics, Mechanical Engineering Department, University of Minho, Campus de Azurém, 4800-058 Guimarães, Portugal
[b] UNESP - São Paulo State University, School of Engineering, Post-Graduation Program in Mechanical Engineering, Av. Brasil, 56, Ilha Solteira, SP 15385-000, Brazil
[c] UNESP- São Paulo State University, Câmpus of São Joãoda Boa Vista, São João da Boa Vista, Brazil
[d] IN+, Center for Innovation, Technology and Policy Research, Instituto Superior Técnico, Universidade de Lisboa. Av. Rovisco Pais, 1049-001 Lisboa, Portugal
[e] CINAMIL—Centro de Investigação Desenvolvimento e Inovação da Academia Militar, Academia Militar, Instituto Universitário Militar, Rua Gomes Freire, 1169-203 Lisboa, Portugal
[f] CEFT, Transport Phenomena Research Center, Porto University Engineering Faculty (FEUP), R. Dr. Roberto Frias, 4200-465 Porto, Portugal

ARTICLE INFO

Keywords:
PDMS cell
Thermal conductivity measurement
Nanofluids
Nanoparticles

ABSTRACT

The traditional methods to measure the thermal conductivity of nanofluids (NFs) do not allow the investigation of critical features that affect the NF's heat transfer performance. For instance, during the thermal conductivity measurements, the NF's thermal properties may be subject to several critical features such as sedimentation, aggregation and wall adhesion of NPs. In addition, the measurement cell has severe functional limitations in terms of full cleaning and performing direct visualizations due mainly to design, geometrical and material constraints. These are frequent problems encountered at the transient hot-wire and transient plane source (TPS) methods, two popular techniques often used to measure NF's thermal conductivity. In this way, polydimethylsiloxane (PDMS), due to its unique properties, such as thermal stability and excellent optical transparency, was applied to fabricate an innovative and simple cell that offers a more straightforward and efficient way to clean the NPs deposited on the walls and as a result to avoid any possible sample contaminations.

1. Introduction

During the 19th century, experiments with hot wires instigated the discussion about heat transfer in gases [1]. The studies of conduction in gases and liquids were widely questioned until the rise of the work of James Clerk Maxwell [2,3] and his theoretical model for thermal conductivity. Maxwell also showed the dependence of thermal conductivity on temperature and pressure. After that, the first devices used to measure the thermal conductivity of liquids may have undergone adaptations from those used to measure solids, particles and gases. Today, such equipment used to measure nanofluids' thermal conductivity experimentally is the same equipment used to measure the thermal conductivity of pure liquids.

A large number of devices in the literature are used to measure the thermal conductivity of fluids, and the main operating methods of these commercial apparatuses are divided into steady-state methods and transient-state methods [4]. Steady-state methods comprise parallel-plane and coaxial cylinders, while transient-state methods include transient hot wire, transient plane source, temperature oscillation, laser flash, and the 3ω [4–6]. More details about the main traditional and new techniques used to measure the thermal conductivity of fluids and nanofluids are presented and discussed in a review article by Souza et al. [6].

In the present work, it was used one of the most popular methods to measure the thermal conductivity of solid materials and fluids, i.e., the hot disk transient plane source (TPS) method. This system is based on the transient plane source technique, where a disk-shaped sensor works as a heat source and temperature sensor [6,7]. In order to measure the thermal conductivity of liquids, the equipment has a cell, i.e., a reservoir, manufactured exclusively for this purpose [6,7]. Inside, the liquid receives a low heating flow to avoid the convection of the liquid. The quantity of fluid volume is also an important parameter when obtaining experimental data since small volumes involved under large areas of insulation tend to prevent heat exchange with the external environment.

Adding nanoparticles in a base fluid, such as water, glycol, oils,

* Corresponding author.
E-mail address: reinaldo.souza@tecnico.ulisboa.pt (R.R. Souza).

https://doi.org/10.1016/j.tsep.2023.101926
Received 20 January 2023; Received in revised form 20 May 2023; Accepted 22 May 2023
Available online 26 May 2023

Nomenclature

–	specific heat, (J/kg•K)
–	Brownian diffusion coefficient, (m^2/s)
–	thermal conductivity, (W/m•K)
–	Boltzmann constant, (J/K)
–	average radius of NPs clusters, (m)
–	radius kapton sensor, (mm)
–	temperature, (°C)

GREEK LETTERS

ρ	mass density, (kg/m^3)
μ	dynamic viscosity, (Pa•s)
φ	particle volume concentration, (w/v%)

SUBSCRIPTS

bf	base fluid
nf	nanofluids
np	nanoparticles

among others, culminates in forming these colloidal mixtures called nanofluids [9]. Unlike pure liquids, the reservoirs where the nanofluids will be placed can be subject to the adhesion of nanoparticles on their internal walls, impairing the reproducibility of the measurements and making them unfeasible/contaminating the experimental measurements.

The preparation of nanofluids in order to obtain the experimental measurements of their thermal conductivity is crucial for the repeatability of the data; depending on the conditions of the tests, measurements can show large fluctuations in the values. Controlling all preparation parameters and test conditions can be one of the reasons for controversial results often shown in the literature [6,9,10] and the difficulties in replicating equivalent nanofluids, as highlighted by [11]. In order to prevent the nanoparticle's deposition in the sensor during experimental measurements of thermal conductivity, influencing the quality of the tests, the nanofluid must be remixed using an ultrasonic bath to ensure homogeneity and prevent any possible precipitation. Another important aspect is to control the temperature of the sample, minimizing the heat exchange with the external environment as much as possible since the temperature influences the thermal conductivity of nanofluids [10,12–14]. For this reason, due to its unique properties, polydimethylsiloxane (PDMS) is a natural choice to place the nanofluid due to its low thermal conductivity, around 0.16 W/m • K at room temperature [15–22]. In addition, PDMS has excellent optical transparency, is a lightweight and corrosion-resistant elastomer, and is a suitable matrix for thermal management materials due to its good flexibility and compressibility [12,15,16,18,20,22]. Simple to manufacture, the PDMS can be easily adapted to the desired shape since when left for a reasonable period on a surface, it takes the entire shape of that, covering it and molding itself and in this way reproducing all its imperfections. Furthermore, the preparation of PDMS resin is a simple procedure that does not require clean rooms or specialized personnel and consists of a mixture of prepolymer plus a curing agent, which can be more or less flexible according to the adopted proportions [18,20].

This work presents an innovative and straightforward PDMS cell to be used in a hot disk TPS method to measure the thermal conductivity of nanofluids. Simple to manufacture and maintain, the nanofluid reservoir made of PDMS is a promising alternative that allows the full and easy filling of the cell, perfect cleaning and isolation, tasks not possible by most traditional cells. Thus, the main objective of the current work is to perform a detailed description of the proposed PDMS cell. Moreover, a brief discussion of the results obtained for the thermal conductivity of three selected nanofluids is presented.

2. Materials

2.1. Hot Disk TPS 2500S

From the transient plane source equipment (TPS), it is possible to obtain information on thermal conductivity, thermal diffusivity, and the specific heat per unit volume of the material under study, having reached ISO 22007–2, according to the manufacturer [8]. The technique uses a flat heated sensor and, according to the manufacturer, is commonly known as a Hot Disk Thermal Constant Analyzer because of its shape. Also, according to the manufacturer's manual, the TPS 2500S equipment allows measuring thermal conductivity values between 0.005 and 1800 W/m • K, with reproducibility usually better than 1% and accuracy better than 5%, being able to use the standard isotropic measurement module and the components.

For measuring the thermal conductivity of liquids, the Hot Disk flat sensor is placed between two parts of the sample using the manufacturer's cell (details of such a cell can be seen in section 2.3 of the current work). The Hot Disk flat sensor can be used as a heat source and dynamic temperature sensor.

2.2. Temperature and heat flux sensor

Hot Disk sensors use thin polyimide films (Kapton®) with thicknesses ranging from 12.7 μm to 25 μm when used at cryogenic temperatures up to 300 °C; this gives a total sensor thickness between 60 and 80 μm. For temperature measurements up to 1000 °C, special Mica insulation is employed. This insulation material is thicker (about 0.1 mm), meaning the sensor's total thickness is about 0.25 mm. The double spiral sensor is etched into a thin nickel foil with an electrically conductive pattern. Nickel foil is chosen because of its known high temperature coefficient of resistance. The conductive pattern is supported by lamination between two thin layers of electrically insulating material.

In this study, the Hot Disk 5501 F1 sensor with Kapton® isolation was used, Fig. 1. The sensor has an outer radius, r_{Hot}, of 10 mm and an inner radius, r_{Kapton}, of 6.4 mm (spiral). Four electrical connections exist for the double spiral on the sensor (two for carrying the heating current and two for controlling the voltage drop). The design of the TPS 2500S equipment is adjusted to measure resistance variations during transient heating of the sample under investigation.

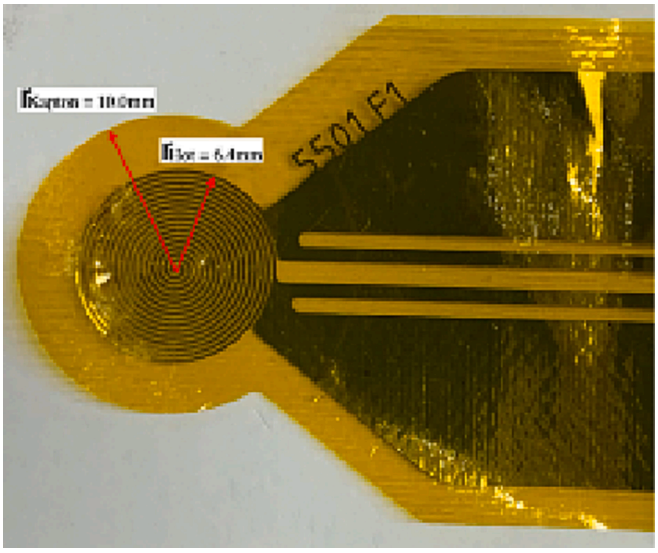

Fig. 1. Sensor Hot Disk 5501 F1 with Kapton® isolation.

2.3. Traditional cell for measuring the thermal conductivity of liquids

Fig. 2 shows the traditional cell frequently used to measure the thermal conductivity of liquids [8]. The liquid is placed in a small cell, separated into two parts, keeping to a minimum the distance between the sensor and the sample to avoid convection during measurements, Fig. 2b and 2c. Furthermore, the cell guarantees a stable temperature due to the relatively large metal volume; evaporation is also avoided since no liquid is exposed to air. The liquid is inserted into the cell through two inlet pipes; each one is responsible for filling the cell that, after being closed, is located between the sensor. A third pipe serves as an air outlet, ensuring the cell is filled only with the liquid to be evaluated. To further control the temperature of the tests, it is recommended to immerse the entire assembly (Fig. 2a) in a thermal bath.

2.4. Design of the proposed PDMS cell

The rapid prototyping technique, consisting of a 3D printing model Dremel 3D45, was used for the mold design. The materials used for printing were Polylactic Acid (PLA) and Polyethylene terephthalate with Glycol (PETG). After obtaining the PLA template, Fig. 3a, the PDMS Sylgard 184 was used to obtain the new cell, Fig. 3b. The cell has a spherical internal shape with a 12.5 mm radius and holds a total volume of 8.0 ml of liquid, with the two parts coupled. One of the parts, the upper one, with 1.0 mm diameter, is used to place the liquid using a syringe with a needle. The external shape of each of the parts is cylindrical, with a height of 25.0 mm.

The preparation of the PDMS resin consists of a mixture of prepolymer and curing agent, which volume depends on the desired flexibility level (in the current study, a ratio of 10:1 was used). The two parts are placed in a container where they are mixed and stirred for 5 min; then, the mixture goes through a degassing process with a vacuum pump. In this step, the compound bubbles are removed and the mixture can be placed in the mold. PDMS cure time at room temperature is 48 h [18,23]. After complete curing, the PLA mold is removed, obtaining the parts as shown in Fig. 3b.

3. Measurement procedures

3.1. PDMS cell configuration

This sub-section describes the PDMS cell configuration steps to perform the experimental measurements. The PDMS cell is divided into two symmetrical parts. One has an opening in its center, which is used to insert the nanofluid using a syringe. The following procedure was carried out:

(i) The fully enclosed PDMS base was placed in the center of the manufacturer's stainless-steel support, the same used to perform thermal conductivity measurements of solids, Fig. 4a;
(ii) A syringe inserts the nanofluid into the cell (4.0 ml of fluid is needed). Once the bottom portion of the cell is filled with the syringe, the sensor is inserted. The operator must place the Hot Disk sensor, ensuring it is centralized with the manufacturer's support and the base made of PDMS, Fig. 4b. It is recommended to use the support screw as a guide;
(iii) The PDMS with the orifice must be joined to the base; the screw of the manufacturer's stainless-steel support must be removed, and its opening must be used as a guide for the syringe to access the orifice, Fig. 4c;
(iv) The top of the cell, which contains the hole, is then placed on the bottom base and the syringe is used again to fill the remaining portion of the cell. An additional 4.0 ml of fluid is necessary. The operator must complete the top of the set by holding the top of the PDMS until the end of filling and tightening the center screw. It is necessary to ensure that no air is presented in the system and that a syringe can be used to remove it, Fig. 4c. Then, the center screw is threaded into the bracket to couple with the PDMS on top of the cell, Fig. 4d. Finally, the insulation of the entire assembly should be made using the manufacturer's steel cover (more details can be found at [8]).

3.2. Device verification and calibration procedure

In order to ensure that the thermal conductivity values of nanofluids are reliable, it is recommended to calibrate the experimental apparatus with traditionally known fluids. According to [24], to carry out this step, it is recommended to use fluids where the thermal conductivity uncertainty of these fluids is about 1.5%. The authors suggest deionized water, glycerol anhydrous, and n-heptane. In the current study, the device was calibrated using deionized water, ethylene glycol, and glycerin (glycerol). Table 1 compares the thermal conductivity value based on experimental measurements with values found in the literature.

The calibration procedure consists of 10 measurements for each fluid (only 5 are shown in Table 1). All tests were performed at a temperature of 22 °C ± 0.4 °C. Table 2 shows the standard conditions adopted for the calibration tests. The short measurement times and low heating powers are necessary to avoid convection heat transfer; 5 min interval between one measurement and another was established to guarantee thermal equilibrium. Regarding the heating power, the manufacturer recommends that heating power must be supplied to acquire a suitable total temperature increase, typically 2–5 K. It is worth mentioning that the sample thermal conductivity affects how much power should be used.

Before tests, two procedures were adopted to control the temperature of the samples. First, the room temperature control is carried out where the Hot Disk TPS 2500S equipment is located. Second, a thermal

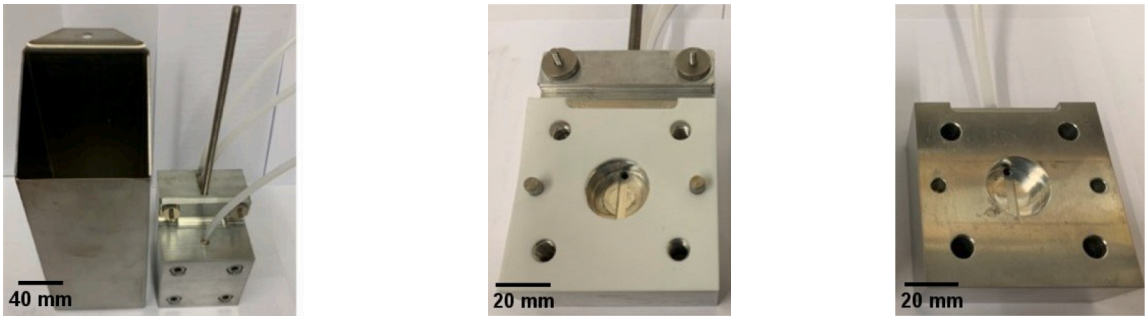

Fig. 2. A) general view of the manufacturer's equipment to measure the thermal conductivity of liquids; b and c) internal details showing the cells and liquid filling openings.

Fig. 3. A) 3d printed mold to perform the PDMS gravity casting process; b) PDMS cell to measure the NFs thermal conductivity.

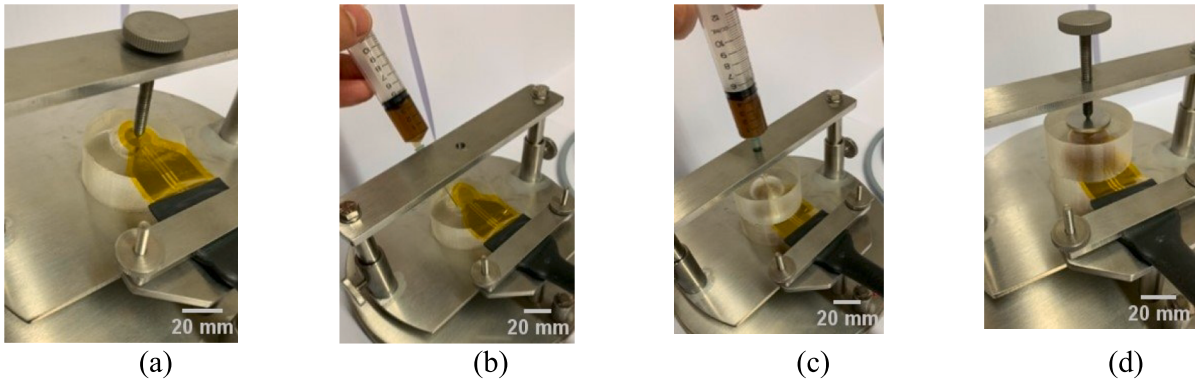

Fig. 4. Procedure to measure the thermal conductivity of nanofluids using the PDMS cell.

Table 1
Device calibration using three different fluids with known thermal conductivity values.

n° of measurements	DI-water (0.6060[1]) [W/m • K]	Ethylene glycol (0.2540[2]) [W/m • K]	Glycerin (0.2860[3]) [W/m • K]
1	0.5920	0.2532	0.2879
2	0.6112	0.2542	0.2866
3	0.6174	0.2553	0.2891
4	0.6051	0.2571	0.2923
5	0.6099	0.2540	0.2904
Average value	**0.6071**	**0.2547**	**0.2873**
$MAE=\frac{1}{N}\sum_{i=1}^{N}\left\|\frac{theo-exp}{theo}\right\|$	±0.18%	±0.29%	±0.13%

[1] Reference data obtained from the Incropera *et al.* [25] at 22 °C; [2]Reference data obtained from the Haynes [26] at 25 °C; [3]Reference data obtained from the Çengel & Ghajar [27] at 20–30 °C.

Table 2
Standard conditions adopted for each calibration test.

Parameters of measurement	DI-water	Ethylene glycol	Glycerin
Heating power [mW]	100	300	300
Measurement time [s]	3	4	4
Points intervals	[10–181]	[30–193]	[30–193]

bath keeps the samples at a constant temperature. For the tests with nanofluids, additional care was taken. Due to the nanoparticle's sedimentation possibility, which could compromise the repeatability of the tests, the samples containing the colloidal mixtures were left for 1 h in an ultrasonic bath immediately before the measurements.

During the calibration tests and the thermal conductivity measurement of the nanofluids, the PDMS cell is coupled to the stainless-steel support and the manufacturer's data acquisition system; the results are recorded on a desktop computer, as shown in Fig. 5.

The nanofluids were prepared using the two-step method [7,28], where the nanoparticles are obtained and then added to the base fluid according to the desired concentrations. Due to the nanoparticle's sedimentation within the nanofluid, which could compromise the repeatability of the tests, the samples containing the colloidal mixtures were left for 2 h in an ultrasonic bath immediately before the measurements. We adopted the same protocol performed by Souza et al. [7]. Table 3 shows the main relevant physical properties of the nanoparticles used in this study.

Finally, the measurements obtained from the PDMS cell were compared with the commercial cell provided by the manufacturer and the results are presented in Table 4. These results are compared with those obtained with our cell in the value of the MAE. Overall, the experimental measurements conducted with the PDMS cell have produced better results in all cases. Furthermore, an additional difficulty was encountered with the commercial cell when testing fluids with high viscosity, such as glycerin. By using the commercial cell, obtaining accurate results was challenging as it was hard to ensure that the cell was filled entirely and free of any air bubbles that are likely to interfere with the sensor and, consequently, compromise the reliability of the measurements.

3.3. Theoretical models to predict the thermal conductivity of nanofluids

The values obtained experimentally were also compared with three theoretical models for thermal conductivity obtained from the literature, as shown in Table 5:

In all expressions presented in Table 5, k_{np}, k_{bf} and φ represent the thermal conductivity of the nanoparticles (NPs), the thermal conductivity of the base fluid (BF) and the concentrations of the NPs, respectively. In Hamilton & Crosser model [29], n represents a parameter

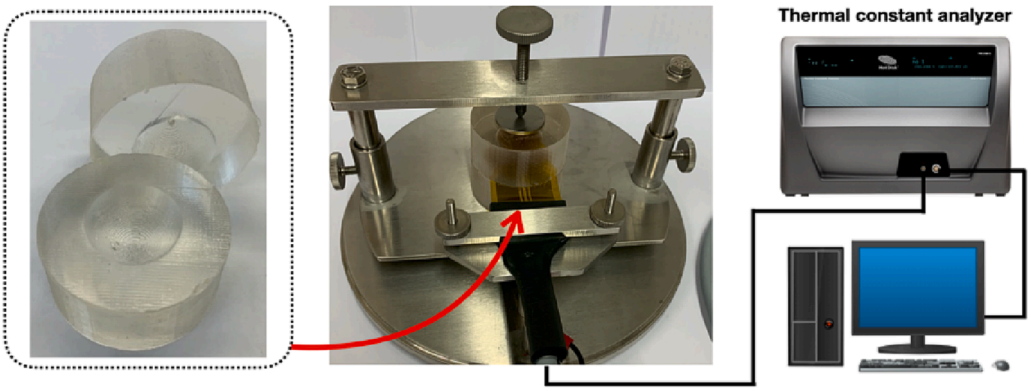

Fig. 5. PDMS cell coupled to the stainless-steel support and the Hot Disk TPS 2500S data acquisition system.

Table 3
Physical properties of the nanoparticles analyzed in the current study.

	*Al_2O_3	Fe_3O_4	*Fe_3O_4@PAA
Physical property	Commercial	Oxide reduction process	Synthesized by hydrothermal method
Size [nm]	<50	160 ± 10	5.0 ± 1.1
color	White	dark brown	dark brown
ρ[kg/m^3]	3900	5170	5170
c_p[J/kgK]	779	670	670
k[W/m • K]	36	6	6

* Data obtained from [7] at 25 °C.

Table 5
Theoretical models for the thermal conductivity of liquids.

Model	Mathematical expression	Remarks
Maxwell [29]	$k_{nf_{Maxwell}} = k_{bf}\left[\frac{k_{np}+2k_{bf}+2\varphi(k_{np}-k_{bf})}{k_{np}+2k_{bf}-2\varphi(k_{np}-k_{bf})}\right]$	Recommended for spherical particles
Hamilton & Crosser [29]	$k_{nf_{H\&C}} = k_{bf}\left[\frac{k_{np}+(n-1)k_{bf}-\varphi(n-1)(k_{bf}-k_{np})}{k_{np}+(n-1)k_{bf}+\varphi(k_{bf}-k_{np})}\right]$	Recommended for two-component systems of different particle shapes and sizes
Xuan [30]	$k_{nf_{Xuan}} = k_{nf_{Maxwell}} + \frac{1}{2}\rho_{nf}c_{p_{np}}\varphi\sqrt{2D_B}$	It takes into account the Brownian motion of particles

related to the particle shape. In other words, it is a form factor and is determined considering the sphericity of the particle, w, being, for example, for a sphere, $w = 3$, or for a cylinder, $w = 0.5$, which allows obtaining the value of n according to the expression:

$$n = \frac{3}{w} \tag{4}$$

In the Xuan model [27], the density and specific heat were obtained through the following expressions [31]:

$$\rho_{nf} = \rho_{np}\varphi + \rho_{bf}(1-\varphi) \tag{5}$$

where ρ_{np} represents the density of the NPs and ρ_{bf} represents the density of the BF, respectively.

$$c_{p_{nf}} = \frac{\varphi\rho_{np}c_{p_{np}} + (1-\varphi)\rho_{bf}c_{p_{bf}}}{\rho_{nf}} \tag{6}$$

In order to obtain the specific heat of the nanofluids, $c_{p_{nf}}$:

where $c_{p_{bf}}$ corresponds to the specific heat of BF, $c_{p_{np}}$ corresponds to the specific heat of NPs. Finally, D_B, the Brownian diffusion term is obtained by:

$$D_B = \frac{k_B T}{6\pi\mu_{bf} r_c} \tag{7}$$

This term includes the random motion effect of the NPs in the BF, where: T corresponds to the temperature of the fluid, r_c corresponds to the mean radius of the NPs (or clusters), k_B corresponds to the Boltzmann constant and μ_{bf} represents the dynamic viscosity of the BF.

4. Results and discussion

For the experimental measurement of the thermal conductivity of nanofluids, three types of samples were used: commercial alumina nanoparticles (Al_2O_3), iron oxide nanoparticles (Fe_3O_4) produced through an oxide-reduction process, and iron oxide nanoparticles (Fe_3O_4@PAA) manufactured through a surface coating process in order to make them highly stable, both produced in the laboratory. Details on the manufacturing process of the nanofluids analyzed in the current work can be found in [7,32–34]. Three concentrations by weight were used, 0.01%, 0.05% and 0.1%. Following the same procedure adopted during the device's calibration, 10 experimental measurements were performed (five values are shown in Table 6).

The standard conditions adopted for each nanofluid, regardless of the mass concentration, were:

- For the Al_2O_3 and Fe_3O_4@PAA was used a heating power of 25 mW, 3 s of time and 10–190 points intervals;
- For the Fe_3O_4 was adopted a heating power of 235 mW, 1 s of time and 6–200 points intervals.

From the results presented in Table 6, one may observe that both nanofluids obtained from conventional nanoparticles (Al_2O_3 and Fe_3O_4) increase the thermal conductivity with the mass concentration. However, the thermal conductivity values are highest when using the hydrothermal method to produce the nanofluids (Fe_3O_4@PAA); for a concentration of 0.01%, the Fe_3O_4@PAA/water nanofluid presents the highest measured thermal conductivity value. As shown in [7], this can be a very positive aspect in applications of heat transfer devices since reducing the nanoparticles concentration in a nanofluid reduces the costs of these mixtures.

Table 7 compares the experimental results for the thermal conductivity of the nanofluids analyzed in the current work with theoretical models presented in Table 5. The mean absolute error (MAE = $\frac{1}{N}\sum_{i=1}^{N}\left|\frac{theo-exp}{theo}\right|$) was used to measure the accuracy of a given model.

For conventional nanofluids, the thermal conductivity increased with an increase in the mass concentration, even for low values of the mass concentrations. Moreover, the experimental values agree well with the models from the literature (Table 5), with an MAE of up to 3.4%. For the nanofluid made from the hydrothermal synthesis process, it is

Table 6
Experimental thermal conductivity [W/m • K] values for nanofluids with different mass concentrations.

n° of measurements	Al_2O_3			Fe_3O_4			Fe_3O_4@PAA		
	0.01%	0.05%	0.1%	0.01%	0.05%	0.1%	0.01%	0.05%	0.1%
1	0.6051	0.6297	0.6272	0.5989	0.6152	0.6049	0.6412	0.6493	0.6438
2	0.6294	0.6212	0.6291	0.6053	0.6113	0.6141	0.6335	0.6382	0.6415
3	0.6070	0.6158	0.6290	0.6061	0.6081	0.6122	0.6334	0.6398	0.6411
4	0.6202	0.6276	0.6252	0.5940	0.5940	0.6116	0.6433	0.6469	0.6485
5	0.6018	0.6197	0.6266	0.6079	0.6103	0.6131	0.6397	0.6429	0.6451
Average value	**0.6127**	**0.6228**	**0.6274**	**0.6024**	**0.6078**	**0.6112**	**0.6382**	**0.6434**	**0.6440**

Table 7
Comparison between experimental thermal conductivity [W/m • K] values and theoretical models from the literature.

	Al_2O_3			Fe_3O_4			Fe_3O_4@PAA		
	0.01%	0.05%	0.1%	0.01%	0.05%	0.1%	0.01%	0.05%	0.1%
Maxwell model	0.6062	0.6072	0.6093	0.6062	0.6069	0.6078	0.6062	0.6069	0.6078
MAE	**1.07%**	**2.57%**	**2.97%**	**0.63%**	**0.15%**	**0.56%**	**5.28%**	**6.02%**	**5.96%**
H & C model	0.6061	0.6063	0.6069	0.6061	0.6063	0.6065	0.6061	0.6063	0.6065
MAE	**1.09%**	**2.72%**	**3.37%**	**0.61%**	**0.25%**	**0.77%**	**5.30%**	**6.12%**	**6.18%**
Xuan's model	0.6069	0.6104	0.6148	0.6066	0.6090	0.6119	0.6085	0.6185	0.6231
MAE	**0.96%**	**2.03%**	**2.04%**	**0.69%**	**0.20%**	**0.11%**	**4.88%**	**4.25%**	**3.36%**

evident that the methodology adopted to prepare the solutions affects the thermal conductivity. It is possible to notice that the values obtained experimentally, for this case, tend to deviate more from the theoretical models from the literature.

5. Future directions

The design of the new PDMS cell opens up discussions for adaptations and future works. Characteristics of the tested material, such as its insulating property, optical properties, and ease of fabrication and conformation, allow cell adaptation to enable visualization of microfluidic and nanofluidic sedimentation during thermal property measurements. For instance, the possibility of adapting the PDMS cell for instruments such as Dynamic Light Scattering (DLS) can be explored. Heat exchangers can also be incorporated within the cell structure to control the temperature of the sample under investigation.

In order to improve the visualization of the samples, a slight modification can be easily performed on the PDMS cell, as shown in Fig. 6. Fig. 6a and 6b present the 3D drawing and the manufactured PDMS cell, respectively. For instance, the creation of a cavity at the PDMS cell will improve the visualization of any possible sedimentation that may occur during the thermal measurements, as shown in Fig. 6c. Furthermore, it is possible to verify the presence of the air bubbles when analyzing liquid samples with high viscosity, such as glycerine (see Fig. 6d), allowing researchers to eliminate the bubbles and, in this way, minimizing some possible measurement errors.

6. Conclusions

This work presents an innovative and straightforward PDMS cell to measure the thermal conductivity of nanofluids (NFs) through a transient plane source (TPS) method. Due to its excellent optical transparency, the PDMS cell has the unique ability to perform direct visualizations. In addition, this cell is simple to handle, allowing the verification/elimination of air bubbles that may appear within the cell and, in this way, eliminating this potential source of error. Unlike the traditional cells, which have internal tubes that are not accessible, this novel PDMS cell comprises two separate parts, which guarantees the complete cleaning of the cell after the tests avoiding any possible sample contamination. Moreover, PDMS is a material with low thermal conductivity and, as a result, allows natural insulation that avoids heat exchange with the external environment. In order to carry out the thermal conductivity measurements, it is only required 8.0 ml of sample, which allows the use of low values of heat flow through the sensor/analyzer, ensuring the elimination of convection during the tests. Note that this amount of sample can be reduced without compromising the

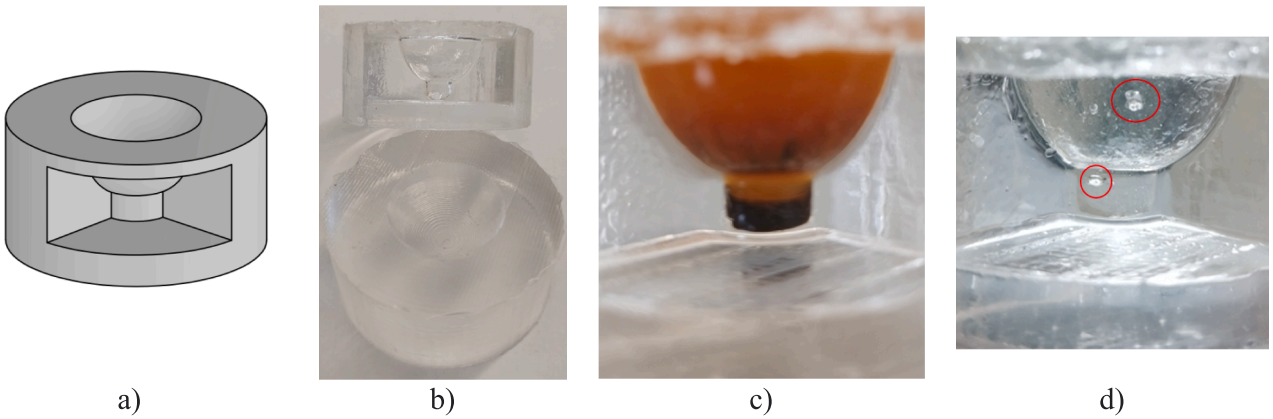

Fig. 6. A) 3d drawing of the modified pdms cell; b) manufactured pdms cell; c) visualization of the sedimentation in a nanofluid with a high concentration of nps; d) visualization of air bubbles in glycerin.

thermal conductivity measurements.

The validation of the PDMS cell was performed using three fluids with known thermal conductivity values, DI-water, ethylene glycol and glycerin, showing satisfactory results as compared to theoretical values (±0.18%, ± 0.29% and ± 0.13%, respectively), ensuring the reliability of the proposed device and equipment.

Regarding the experimental measurements of the NFs thermal conductivity, it was used commercial alumina nanoparticles (Al_2O_3), iron oxide nanoparticles (Fe_3O_4), and polyacrylic acid-bound iron oxide magnetic nanoparticles (Fe_3O_4@PAA). The experimental thermal conductivity values for the conventional NFs agree well with the literature models, with an MAE of up to 3.4%. For Fe_3O_4@PAA, the experimental thermal conductivity values tend to deviate from the theoretical models due to the methodology adopted to prepare such solutions.

Although the PDMS cell was tested in a TPS method in the present work, it is worth mentioning that the proposed PDMS cell can also be used in other thermal conductivity methods by performing simple design modifications. Additionally, due to the ability to perform direct visualizations, the proposed PDMS cell combined with a high-speed video microscopy system has an enormous potential to investigate critical features that affect the NFs heat transfer performance, such as sedimentation, aggregation and clusters of NPs.

CRediT authorship contribution statement

R.R. Souza: Conceptualization, Methodology, Validation, Data curation, Writing – original draft, Writing – review & editing. **F.M. Sá Barbosa:** Conceptualization, Methodology, Validation, Data curation, Writing – review & editing. **G. Nobrega:** Validation, Data curation, Writing – review & editing. **E.M. Cardoso:** Writing – original draft, Writing – review & editing, Resources, Funding acquisition. **J.C.F. Teixeira:** Writing – review & editing, Resources, Funding acquisition. **A. S. Moita:** Writing – review & editing, Supervision, Resources, Funding acquisition. **R. Lima:** Conceptualization, Methodology, Writing – original draft, Writing – review & editing, Supervision, Resources, Funding acquisition.

Declaration of Competing Interest

The authors declare that they have no known competing financial interests or personal relationships that could have appeared to influence the work reported in this paper.

Data availability

Data will be made available on request.

Acknowledgments

This work has been funded by FCT/MCTES (PIDDAC) through the base funding from the following research units: UIDP/50009/2020- FCT and UIDB/50009/2020- FCT, UIDB/00532/2020, UIDB/04077/2020 and UIDP/04077/2020. The authors are also grateful for FCT funding through 2022.03151.PTDC, PTDC/EME-TED/7801/2020, POCI-01-0145-FEDER-016861, POCI-01-0145-FEDER-028159, funded by COMPETE2020, NORTE2020, PORTUGAL2020, and FEDER. Glauco Nobrega was supported by the doctoral Grant PRT/BD/153088/2021, financed by the Portuguese Foundation for Science and Technology (FCT), under MIT Portugal Program. The authors are also very grateful to Eng. Carlos Alberto Costa (UMinho) for the technical assistance provided to this research work, Dr. M. Bañobre-López and Dr. V. Faustino (INL) for providing us the Fe3O4@PAA nanoparticles. E. M. Cardoso also acknowledges the financial support from the National Council of Technological and Scientific Development of Brazil (CNPq grant number 458702/2014-5 and 309848/2020-2) and FAPESP (grant number 2013/15431-7, 2019/02566-8, and 2022/03946-1). Authors also acknowledge to Exercito Português for the support through projects CINAMIL Desenvolvimento de Sistemas de Gestão Térmica e Climatização de equipamento NBQ and COOLUAV - Sistema de arrefecimento da componente eletrónica e baterias em veículos militares não tripulados

References

[1] M.J. Assael, K.D. Antoniadis, W.A. Wakeham, Historical evolution of the transient hot-wire technique, Int. J. Thermophys. 31 (2010) 1051–1072, https://doi.org/10.1007/s10765-010-0814-9.

[2] J.C.M. M.A., II. Illustrations of the dynamical theory of gases, London, Edinburgh, Dublin Philos. Mag. J. Sci. 20 (1860) 21–37. doi:10.1080/14786446008642902.

[3] J.C.M. M.A., V. Illustrations of the dynamical theory of gases.—Part I. On the motions and collisions of perfectly elastic spheres, London, Edinburgh, Dublin Philos. Mag. J. Sci. 19 (1860) 19–32. doi:10.1080/14786446008642818.

[4] I. Gonçalves, R. Souza, G. Coutinho, J. Miranda, A. Moita, J.E. Pereira, A. Moreira, R. Lima, Thermal Conductivity of Nanofluids: A Review on Prediction Models, Controversies and Challenges, Appl. Sci. 11 (2021), https://doi.org/10.3390/app11062525.

[5] A.R. Sajadi, M.H. Kazemi, Investigation of turbulent convective heat transfer and pressure drop of TiO2/water nanofluid in circular tube, Int. Commun. Heat Mass Transf. 38 (2011) 1474–1478, https://doi.org/10.1016/j.icheatmasstransfer.2011.07.007.

[6] R.R. Souza, V. Faustino, I.M. Gonçalves, A.S. Moita, M. Bañobre-López, R.A. Lima, Review of the Advances and Challenges in Measuring the Thermal Conductivity of Nanofluids, Nanomaterials. 12 (2022) 2526, https://doi.org/10.3390/nano12152526.

[7] R.R. Souza, V. Faustino, J.D. Oliveira, I.M. Gonçalves, J.M. Miranda, A.S. Moita, A. L.N. Moreira, J.C.F. Teixeira, M. Bañobre-López, R. Lima, A novel and extremely stable nanofluid based on iron oxide nanoparticles: Experimental investigations on the thermal performance, Therm. Sci. Eng. Prog. 26 (2021), 101085, https://doi.org/10.1016/j.tsep.2021.101085.

[8] Hot Disk Thermal Constants Analyser, Instruction Manual, Revision date 2019-10-08., 2019.

[9] R.R. Souza, I.M. Gonçalves, R.O. Rodrigues, G. Minas, J.M. Miranda, A.L. N. Moreira, R. Lima, G. Coutinho, J.E. Pereira, A.S. Moita, Recent advances on the thermal properties and applications of nanofluids: From nanomedicine to renewable energies, Appl. Therm. Eng. 201 (2022), 117725, https://doi.org/10.1016/j.applthermaleng.2021.117725.

[10] G. Nobrega, R.R. de Souza, I.M. Gonçalves, A.S. Moita, J.E. Ribeiro, R.A. Lima, Recent Developments on the Thermal Properties, Stability and Applications of Nanofluids in Machining, Solar Energy and Biomedicine, Appl. Sci. 12 (2022), https://doi.org/10.3390/app12031115.

[11] B. Buonomo, L. Colla, L. Fedele, O. Manca, L. Marinelli, A comparison of nanofluid thermal conductivity measurements by flash and hot disk techniques, J. Phys. Conf. Ser. 547 (2014), https://doi.org/10.1088/1742-6596/547/1/012046.

[12] H.A. Mintsa, G. Roy, C.T. Nguyen, D. Doucet, New temperature dependent thermal conductivity data for water-based nanofluids, Int. J. Therm. Sci. 48 (2009) 363–371, https://doi.org/10.1016/j.ijthermalsci.2008.03.009.

[13] A. Riahi, S. Khamlich, M. Balghouthi, T. Khamliche, T.B. Doyle, W. Dimassi, A. Guizani, M. Maaza, Study of thermal conductivity of synthesized Al2O3-water nanofluid by pulsed laser ablation in liquid, J. Mol. Liq. 304 (2020), https://doi.org/10.1016/j.molliq.2020.112694.

[14] R. Agarwal, K. Verma, N.K. Agrawal, R. Singh, Comparison of Experimental Measurements of Thermal Conductivity of Fe2O3 Nanofluids Against Standard Theoretical Models and Artificial Neural Network Approach, J. Mater. Eng. Perform. 28 (2019) 4602–4609, https://doi.org/10.1007/s11665-019-04202-z.

[15] J. Wei, M. Liao, A. Ma, Y. Chen, Z. Duan, X. Hou, M. Li, N. Jiang, J. Yu, Enhanced thermal conductivity of polydimethylsiloxane composites with carbon fiber, Compos. Commun. 17 (2020) 141–146, https://doi.org/10.1016/j.coco.2019.12.004.

[16] X. Hou, Y. Chen, L. Lv, W. Dai, S. Zhao, Z. Wang, L. Fu, C.-T. Lin, N. Jiang, J. Yu, High-Thermal-Transport-Channel Construction within Flexible Composites via the Welding of Boron Nitride Nanosheets, ACS Appl. Nano Mater. 2 (2019) 360–368, https://doi.org/10.1021/acsanm.8b01939.

[17] J. He, J.R. Sootsman, S.N. Girard, J.-C. Zheng, J. Wen, Y. Zhu, M.G. Kanatzidis, V. P. Dravid, On the Origin of Increased Phonon Scattering in Nanostructured PbTe Based Thermoelectric Materials, J. Am. Chem. Soc. 132 (2010) 8669–8675, https://doi.org/10.1021/ja1010948.

[18] I. Miranda, A. Souza, P. Sousa, J. Ribeiro, E.M.S. Castanheira, R. Lima, G. Minas, Properties and Applications of PDMS for Biomedical Engineering: A Review, J. Funct. Biomater. 13 (2022), https://doi.org/10.3390/jfb13010002.

[19] D. Pinho, B.N. Muñoz-Sánchez, C.F. Anes, E.J. Vega, R. Lima, Flexible PDMS microparticles to mimic RBCs in blood particulate analogue fluids, Mech. Res. Commun. 100 (2019) 18–20.

[20] R. Ariati, F. Sales, A. Souza, R.A. Lima, J. Ribeiro, Polydimethylsiloxane Composites Characterization and Its Applications: A Review, Polym. 13 (2021), https://doi.org/10.3390/polym13234258.

[21] A. Souza, M. S. Souza, D. Pinho, R. Agujetas, C. Ferrera, R. Lima, H. Puga, H., J. Ribeiro, 3D manufacturing of intracranial aneurysm biomodels for flow visualizations: Low cost fabrication processes. Mech. Res. Commun. 107 (2020), 103535.

[22] C. Cardoso, C.S. Fernandes, R. Lima, J. Ribeiro, Biomechanical analysis of PDMS channels using different hyperelastic numerical constitutive models, Mech. Res. Commun. 90 (2018) 26–33, https://doi.org/10.1016/j.mechrescom.2018.04.007.
[23] The Dow CompanyChemical. SYLGARD. 184 Silicone Elastomer Technical Datasheet. Silicone Elastomer Technical Data Sheet 2017., (n.d.).
[24] B. Barbés, R. Páramo, F. Sobrón, E. Blanco, C. Casanova, Thermal conductivity measurement of liquids by means of a microcalorimeter, J. Therm. Anal. Calorim. 104 (2011) 805–812, https://doi.org/10.1007/s10973-010-1169-y.
[25] F.P. Incropera, Fundamentals of heat and mass transfer : Frank P. Incropera ... [et al.]., 6th ed., Wiley, Hoboken, N.J, 2007.
[26] W.M. Haynes, CRC Handbook of Chemistry and Physics. 91st ed. Boca Raton, FL: CRC Press Inc., 2010-2011, p.6-240.
[27] A.J. Çengel, Y.A. and Ghajar, Heat and Mass Transfer: Fundamentals & Applications. McGraw-Hill, New York, 924. 2011.
[28] Z. Haddad, C. Abid, H.F. Oztop, A. Mataoui, A review on how the researchers prepare their nanofluids, Int. J. Therm. Sci. 76 (2014) 168–189, https://doi.org/10.1016/j.ijthermalsci.2013.08.010.
[29] B. Lamas, B. Abreu, A. Fonseca, N. Martins, M. Oliveira, Critical analysis of the thermal conductivity models for CNT based nanofluids, Int. J. Therm. Sci. 78 (2014) 65–76, https://doi.org/10.1016/j.ijthermalsci.2013.11.017.
[30] Y. Xuan, Q. Li, W. Hu, Aggregation structure and thermal conductivity of nanofluids, AIChE J. 49 (2003) 1038–1043, https://doi.org/10.1002/aic.690490420.
[31] C. Pang, J.W. Lee, Y.T. Kang, Review on combined heat and mass transfer characteristics in nanofluids, Int. J. Therm. Sci. 87 (2015) 49–67, https://doi.org/10.1016/j.ijthermalsci.2014.07.017.
[32] Y. V Kolen'ko, M. Bañobre-López, C. Rodríguez-Abreu, E. Carbó-Argibay, A. Sailsman, Y. Piñeiro-Redondo, M.F. Cerqueira, D.Y. Petrovykh, K. Kovnir, O.I. Lebedev, J. Rivas, Large-Scale Synthesis of Colloidal Fe3O4 Nanoparticles Exhibiting High Heating Efficiency in Magnetic Hyperthermia, J. Phys. Chem. C. 118 (2014) 8691–8701. doi:10.1021/jp500816u.
[33] R.R. de Souza, V. Faustino, I.M. Gonçalves, J.M. Miranda, A.S. Moita, A.L. N. Moreira, M. Bañobre-López, R. Lima, Experimental Studies of the Sedimentation, Stability and Thermal Conductivity of Two Different Nanofluids, Eng. Proc. 4 (2021), https://doi.org/10.3390/Micromachines2021-09589.
[34] A.P. da Cunha, T.S. Mogaji, R.R. de Souza, E.M. Cardoso, A Method for Measuring Contact Angle and the Influence of Surface-Fluid Parameters on the Boiling Heat Transfer Performance, J. Heat Transfer. 142 (2020), https://doi.org/10.1115/1.4047057.